

# Gate Tunable Josephson Diode in Proximitized InAs Supercurrent Interferometers

Carlo Ciaccia,<sup>1,\*</sup> Roy Haller,<sup>1</sup> Asbjørn C. C. Drachmann,<sup>2</sup> Constantin Schrade,<sup>2</sup>  
Tyler Lindemann,<sup>3,4</sup> Michael J. Manfra,<sup>3,4,5,6</sup> and Christian Schönenberger<sup>1,7,†</sup>

<sup>1</sup>*Quantum- and Nanoelectronics Lab, Department of Physics, University of Basel, 4056 Basel, Switzerland*

<sup>2</sup>*Center for Quantum Devices, Niels Bohr Institute,  
University of Copenhagen, 2100 Copenhagen, Denmark*

<sup>3</sup>*Department of Physics and Astronomy, Purdue University, West Lafayette, Indiana 47907, USA*

<sup>4</sup>*Birck Nanotechnology Center, Purdue University, West Lafayette, Indiana 47907, USA*

<sup>5</sup>*Elmore Family School of Electrical and Computer Engineering,  
Purdue University, West Lafayette, Indiana 47907, USA*

<sup>6</sup>*School of Materials Engineering, Purdue University, West Lafayette, Indiana 47907, USA*

<sup>7</sup>*Swiss Nanoscience Institute, University of Basel, 4056 Basel, Switzerland*

The Josephson diode (JD) is a non-reciprocal circuit element that supports a larger critical current in one direction compared to the other. This effect has gained a growing interest because of promising applications in superconducting electronic circuits with low power consumption. Some implementations of a JD rely on breaking the inversion symmetry in the material used to realize Josephson junctions (JJs), but a recent theoretical proposal has suggested that the effect can also be engineered by combining two JJs hosting highly transmitting Andreev bound states in a Superconducting Quantum Interference Device (SQUID) at a small, but finite flux bias [1]. We realized a SQUID with two JJs fabricated in a proximitized InAs two-dimensional electron gas (2DEG). We demonstrate gate control of the diode efficiency from zero up to around 30% for different flux biases which comes close to the maximum of  $\sim 40\%$  predicated in Ref. [1]. The key ingredient to the JD effect in the SQUID arrangement is the presence of an asymmetry between the two SQUID arms.

## I. INTRODUCTION

A widely used device in semiconductor electronics is the  $p-n$  junction, which is a nonreciprocal element with regards to current flow, able to conduct current primarily in one direction. The presently ongoing rapid scaling of quantum computer chips will require control electronics that operate close to the quantum chip at low temperatures, having low dissipation. These requirements have renewed the question whether there exists a superconducting equivalent of the diode, namely a device that supports a larger supercurrent in one direction than in another: the Josephson Diode (JD).

A conventional Josephson junction (JJ) [2] has a current-phase relation (CPR) that is  $2\pi$ -periodic, and obeys time-reversal symmetry, meaning that  $I(\varphi) = -I(-\varphi)$ . Here  $I(\varphi)$  is the supercurrent and  $\varphi$  the applied phase difference over the junction, also known as the phase bias. These equations show that the supercurrent is zero for  $\varphi = 0$  and for  $\varphi = \pi$ . The simplest incarnation due to Josephson [2] is the sinusoidal CPR where the supercurrent is given by  $I(\varphi) = I_c \sin(\varphi)$  with  $I_c$  the critical current and the ground state at  $\varphi = \varphi_0 = 0$ . Here, obviously, the positive critical current,  $I_c^+ = \max_{\varphi}[I(\varphi)]$  is equal to the negative critical current,  $I_c^- = |\min_{\varphi}[I(\varphi)]|$ . Since the supercurrent is reciprocal, there is no diode effect. However, this is not true for general CPRs [3]. A necessary condition is that time-reversal symmetry is broken by, e.g., a magnetic field or by coupling to built-

in ferromagnetic elements, such that  $I(\varphi)$  is no longer an odd function in  $\varphi$ .

In quantum dot (QD) devices sandwiched in between two superconductors (S), i.e. in S-QD-S junctions, where the QD is in a Kondo state, a quantum phase transition can occur accompanied by a switch in the ground state phase from  $\varphi_0 = 0$  to  $\varphi_0 = \pi$  [4, 5]. Consequently the CPR is shifted by  $\pi$  [6] and such junctions are termed  $\pi$ -junctions. They have also been predicated for S-F-S junctions, where F denotes a ferromagnet [7, 8], and were experimentally studied in various configurations [9–11]. Depending on parameters and value of  $\varphi$ , the CPR may also switch from a zero to a  $\pi$  state and back to zero as a function of  $\varphi$ . Despite the presence of a magnetic field and time-reversal symmetry being broken, these junctions still obey  $I(0) = I(\pi) = 0$ .

A special attention has been captured by the so-called anomalous JJs, also known as  $\varphi_0$  junctions, where the ground state of the junction is shifted to  $\varphi_0$  with  $0 < \varphi_0 < \pi$ , leading to  $I(\varphi_0) = 0$  [12]. They arise in devices where time reversal and chiral symmetry is broken. The latter describes an asymmetry between the spin-up (spin-down) current flowing to the right and the spin-up (spin-down) current flowing to the left. This situation is achieved in multiband conductors with spin-orbit interaction [13–16]. Evidence for  $\varphi_0$  junctions has been found in experiments with nanowires with strong spin-orbit interaction [17] and in planar Josephson junction arrays [18].

It has also been recognized that a diode effect may arise in materials where inversion symmetry is broken [19, 20]. This is, for example, the case for materials that display a magneto-chiral anisotropy. Here, the normal-state re-

\* E-mail: [Carlo.Ciaccia@unibas.ch](mailto:Carlo.Ciaccia@unibas.ch)

† E-mail: [Christian.Schoenberger@unibas.ch](mailto:Christian.Schoenberger@unibas.ch)

sistivity itself depends on the sign of the current density and the sign of the magnetic field [21, 22]. While this is a small effect in normal metals, it can become large at the transition to a superconductor [23–25]. Recently, a large superconducting diode effects was also observed in a 2D NbSe<sub>2</sub> superconductor with applied out-of-plane magnetic field [26] and even in a field-free situation including twisted trilayer graphene [27, 28].

Further studies have also considered, among others, polarized supercurrents, magnetic domain walls, combination of s-wave and p-wave pairing, as well as finite-momentum pairing as the origin of a diode effect [29–31]. Lastly, topological materials with helical edge states can carry supercurrents with a strong diode effect [32–34]. This is evidenced in the highly asymmetric Fraunhofer pattern with the property that  $I_c(B) \neq I_c(-B)$ , where  $B$  is the magnetic field. It has been pointed out that in order to see a diode effect, inversion symmetry should be broken in the material. This later condition can also be rephrased in stating that the supercurrent along the two edges of the crystal should be unequal [32]. Since such a configuration is very much alike a SQUID, one could also say that an asymmetric SQUID will yield a diode effect.

In the 1970s, when superconducting interference devices were studied in great detail using tunnel junctions, point contact structures and Dayem bridges, it was recognized that the critical current of a SQUID can become non-reciprocal [35–38]. The origin was understood to emerge from an asymmetry in the two SQUID arms, but the arms needed to have a non-negligible loop inductance, too. Although the CPR of each single junction was sinusoidal, the CPR became non-reciprocal for the SQUID device due to asymmetric loop inductances. However, in these cases the diode effect was not tunable.

Today, tunable superconductor-semiconductor hybrid devices have become a flourishing research topic [4, 39–42]. In particular, in weak links with an intermediate semiconducting channel, the magnitude of the supercurrent is tunable by local gate electrodes and, in some devices, the shape of the CPR can be tuned from sinusoidal to highly non-sinusoidal. Consequently, these devices provide a platform for the engineering of the diode effect with unprecedented tunability. This has recently been investigated theoretically in Ref. [1]. It has been shown that one can achieve a diode effect combining two asymmetric and non-sinusoidal JJs in a dc-SQUID at finite flux bias.

Junctions which are highly transmissive are known to possess a strongly non-sinusoidal CPR [43, 44]. Thus, it is possible to engineer a two junction circuit that maximizes the superconducting diode effect to the predicated maximum value of  $\sim 40\%$  [1].

In the current work, we use gate-controlled JJs that are fabricated in an InAs 2DEG proximitized by an Al layer that is placed close to the 2DEG [45, 46]. These rather wide junctions contain many channels with a distribution of transmission eigenvalues. The non-sinusoidal character is due to highly transmissive channels that are present

in these devices [47–52]. By tuning the average transmission of the two junctions with the respective gate-voltages we show that we can achieve a diode effect up to 30%. This comes close to the maximum theoretically predicted value [1].

In Sec. II we present the device geometry, the experimental set up and the basic characterization of the individual JJs. The non-reciprocal character of the dc-SQUID with JJs having a non-sinusoidal CPR is then shown in Sec. III. We also define an analytical framework with which we are able to distinguish possible origins of the JD effect. Finally, we discuss the measured gate tunability of the diode efficiency in Sec. IV and end with the conclusion in Sec. V.

## II. DEVICE AND BASIC PROPERTIES

The circuit diagram of the device is shown in Fig. 1a) and a coloured electron-microscopy picture is presented in Fig. 1b). The circuit consists of a dc SQUID formed by two planar JJs realized in a shallow InAs 2DEG proximitized by Al. The 2DEG is obtained from a quantum well grown on an InP substrate embedded in InGa<sub>0.25</sub>As<sub>0.75</sub> layers of which the top layer is 10 nm thick. The stack is terminated with an in-situ grown 10 nm thin Al layer inducing superconductivity in the 2DEG. The SQUID loop and the leads are defined by etching Al and 300 nm into the semiconductor stack. The top JJ<sub>1</sub> and bottom JJ<sub>2</sub> in the two branches of the loop, see schematics in Fig. 1a), are formed by selectively removing the Al in the form of stipes with length  $L = 150$  nm and width  $W_1 = 3$   $\mu\text{m}$  and  $W_2 = 2.5$   $\mu\text{m}$ .

A set of gates,  $V_{G1}$ ,  $V_{G2}$  and  $V_{FG}$ , are used to tune the junctions critical currents. They are made of two Ti/Au layers, isolated from the Al and from each other by hafnium dioxide (HfO<sub>2</sub>) layers.  $V_{G1}$  extends over the whole width of JJ<sub>1</sub>, while  $V_{G2}$  is shaped to gradually deplete JJ<sub>2</sub> laterally, creating a Superconducting Quantum Point Contact (SQPC). An additional gate,  $V_{FG}$ , can be use to fine tune the charge carrier density in the SQPC. Throughout the experiment, we keep  $V_{FG} = 0\text{V}$ .

Our setup sources a current using a 1 M $\Omega$  resistor in series to a dc voltage superposed by a small ac component with frequency  $f = 17.7$  Hz, supplied by a lock-in amplifier. The ac component has an amplitude in current of 5 nA. This current is applied to the source contact of the SQUID on the left with the drain contact on the right side galvanically connected to ground. The SQUID is additionally shunted at the source to ground with a resistor  $R_S = 10$   $\Omega$ . This shunt resistor is directly placed on the sample holder. It has two purposes: a) it limits the maximum voltage that appears over the junction in the normal state, and thus, the heating; and b) it adds damping to the device avoiding hysteretic switching when assessing the critical current in experiments. We measure the differential resistance of

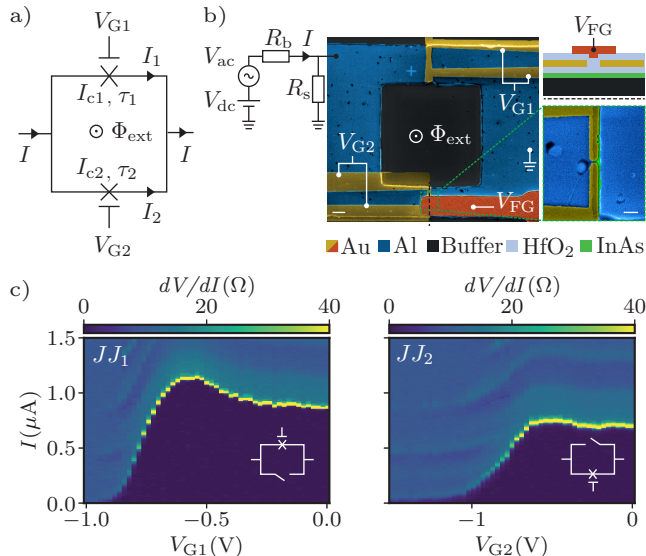


Figure 1. a) Circuit schematic of a dc SQUID threaded by the external flux  $\Phi_{\text{ext}}$ , formed by two gate tunable JJs with non-sinusoidal CPRs with critical currents  $I_{c1}$ ,  $I_{c2}$ , and transparencies  $\tau_1$ ,  $\tau_2$ . b) False-color electron micrograph of the device. The loop consists of a 10 nm Al film (blue) grown on top of an InAs 2DEG (purple). The JJs are defined by selectively removing the Al over 150 nm long stripes on each branch of the loop. Electrostatic gates (yellow and orange) tune the charge carrier density in the junction. We use 15 nm of HfO<sub>2</sub> (light blue) as a gate dielectric. On the right, a zoom-in of JJ<sub>2</sub> is shown. On top, we show a cross-sectional schematic of the gate configuration of JJ<sub>2</sub> along the dashed black line. The scale bar in the main figure is 1  $\mu\text{m}$  and in the zoom-in it is 300 nm. Dc and ac current bias are defined through the voltage drop over a large series resistor with value  $R_b = 1 \text{ M}\Omega$ . The SQUID is shunted to ground with a parallel resistor of value  $R_s = 10 \Omega$ . c) Differential resistance of JJ<sub>1</sub> (left) and JJ<sub>2</sub> (right) as a function of gate voltage and current bias. While one junction is being measured, the other is pinched-off. The top junction has a slightly higher critical current due to the different channel widths of  $W_1 = 3 \mu\text{m}$  and  $W_2 = 2.5 \mu\text{m}$ .

the shunted device using a voltage amplifier and lock-in techniques. In all plots where a measured differential resistance  $dV/dI$  is shown the shunt resistor was not subtracted. The measurements presented in the following were obtained with the SQUID device operating in a dilution refrigerator with a base temperature of  $\sim 50 \text{ mK}$ .

In Fig. 1c) we show the measured differential resistance of JJ<sub>1</sub> (left) and JJ<sub>2</sub> (right) as a function of gate voltage and bias current. In the following, we approximate the critical current  $I_{ci}$  of the  $i$ th-junction,  $i = \{1, 2\}$ , by the current bias value at which we measure the maximum value in differential resistance. Here, the bias current is swept from zero to 1.5  $\mu\text{A}$ , looking at transitions from the superconducting to the normal state. From the measurements we extract  $I_{ci}(V_{Gi})$ . The critical current of both junctions can be tuned from a few nA close to pinch-off at

negative gate-voltages  $V_{G(1,2)} \lesssim -1 \text{ V}$  to approximately 1  $\mu\text{A}$ . The tunability of  $I_c$  is one of the key ingredients of these hybrid semiconductor-superconductor JJs. The other one is its non-sinusoidal character.

In the current work, we will demonstrate that one can obtain a large diode effect by using JJs that have a strong non-sinusoidal CPR. In the short-junction limit, i.e. for junctions with a length  $L$  shorter than the normal metal coherence length  $\xi$ , the zero temperature limit of the supercurrent  $I(\varphi)$  is given by [43]:

$$I(\varphi) = \sum_j \left( \frac{\tau_j e \Delta}{\hbar} \right) \frac{\sin(\varphi)}{\sqrt{1 - \tau_j \sin^2(\varphi/2)}}. \quad (1)$$

Here,  $\tau_j$  is the transmission probability per mode. In multichannel devices with disorder, a universal distribution function of transmission eigenvalues was obtained [47, 53–55]. The distribution is bimodal with many low transmissive channels that contribute little to the current, but also with some channels having a transmission probability close to 1. These high-transmissive channels lead to the overall non-sinusoidal character. This is approximated with a mean transmission probability  $\bar{\tau}$  per channel and written as a single non-sinusoidal CPR given by:

$$I(\varphi) = \frac{I_c}{A_N} \frac{\sin(\varphi)}{\sqrt{1 - \bar{\tau} \sin^2(\varphi/2)}}. \quad (2)$$

For the later discussion of the measurements we introduce here the critical current  $I_c$  of the junction and a unit-less normalization parameter  $A_N$ . The ratio  $I_c/A_N$  is given by  $N\bar{\tau}e\Delta/\hbar$  with  $N$  the number of channels. Note, for the single junction we have  $I(-\varphi) = -I(\varphi)$  and thus  $I_c^+ = I_c^- = I_c$ . It is also seen that for small values of  $\bar{\tau}$  the CPR approaches a sinusoidal dependence. From experimental  $I(\varphi)$  curves, we deduce the critical current  $I_c$  of each junction,  $\bar{\tau}$  and  $A_N$ . Note, that only two parameters are independent. We have measured CPRs of each junction separately by tuning them to an asymmetric SQUID configurations. In a sufficiently asymmetric configuration one can measure the CPR of the weak junction alone when one sweeps the magnetic flux through the loop [44].

As shown in Fig. 1a) the total supercurrent  $I$  across the SQUID is the sum of the currents flowing in both branches  $I_1$  and  $I_2$  through the two JJs:

$$I(\varphi_1, \varphi_2) = I_1(\varphi_1) + I_2(\varphi_2). \quad (3)$$

The two junctions are described by  $I_{c1}, I_{c2}$  and  $\bar{\tau}_1, \bar{\tau}_2$ . The uniqueness of phase around the loop leads to the so-called fluxoid relation (modulo  $2\pi$ )

$$\varphi_1 - \varphi_2 = 2\pi\Phi_{\text{ext}}/\Phi_0 = \varphi_{\text{ext}}, \quad (4)$$

where  $\Phi_{\text{ext}}$  denotes the externally induced flux,  $\Phi_0 = h/2e$  the superconducting flux quantum and  $\varphi_{\text{ext}}$

the respective phase. In this form of the fluxoid relation the loop inductance has been neglected. For a finite loop inductance there is an additional flux contribution which depends on the currents  $I_1$  and  $I_2$  flowing in each arm. It has been shown that asymmetric loop inductances can also induce a superconducting diode effect [38, 56, 57]. To estimate the role of loop inductances in our experiment we perform a full analysis with equations given in the supplemental materials (SM). Taking Eq. 3 and Eq. 4 together yields an effective superconducting junction with a CPR

$$I(\varphi) = I_1(\varphi) + I_2(\varphi - \varphi_{\text{ext}}). \quad (5)$$

For a simple sinusoidal CPR, the addition of the two terms yields a  $\varphi_0$ -junction without a diode effect, even when the two JJ have different critical currents. In the presence of higher order harmonics, which appear for a non-sinusoidal CPR, constructive and destructive interference effects, acting opposite for the two current bias directions, give rise to unequal critical currents  $I_c^+ \neq I_c^-$ , and thus to a diode effect [1].

### III. JOSEPHSON DIODE EFFECT

Fig. 2a) shows the differential resistance of the SQUID as a function of current bias and perpendicular magnetic field  $B_\perp$ , the latter providing the flux  $\Phi_{\text{ext}}$  through the SQUID loop. We have chosen a gate configuration with  $V_{G1} = V_{G2} = 0$  V for which the two critical currents are similar:  $I_{c1} = 0.87 \mu\text{A}$  and  $I_{c2} = 0.67 \mu\text{A}$ . A clear diode effect is visible. For example, at the place of the orange arrow, we obtain  $I_c^+ = 0.64 \mu\text{A}$  and  $I_c^- = 0.4 \mu\text{A}$ .

In this experiment, the current bias is swept from a fully negative current to the maximum positive current. This means that we measure the positive switching current, but on the negative side, we measure what is called the retrapping current value where the device switches from the normal state to the superconducting one. Due to dissipation, the junction can overheat in the normal state giving rise to a hysteresis between the switching and retrapping currents with the retrapping current being smaller in magnitude than the switching current. This would give rise to an artificial diode effect. To exclude this, we have also measured the same plot as in Fig. 2a) but sweeping now fully from positive to negative bias currents. The comparison shows, see SM, that the hysteresis between retrapping and switching currents is small and can be neglected. Physically, this is the case thanks to the low shunt resistant of  $R_s = 10 \Omega$  which limits the voltage over the junction to  $< 25 \mu\text{V}$ , and thus, limits the heating.

Another strong argument against an artificial effect is seen in Fig. 2a) when one looks at the switching values at the place of the red arrow, where  $I_c^+ = 0.44 \mu\text{A}$  and  $I_c^- = 0.6 \mu\text{A}$ . Here, the sign of the diode effect is reversed,  $I_c^+ < I_c^-$ . This cannot be explained by a hysteresis between the switching and retrapping currents.

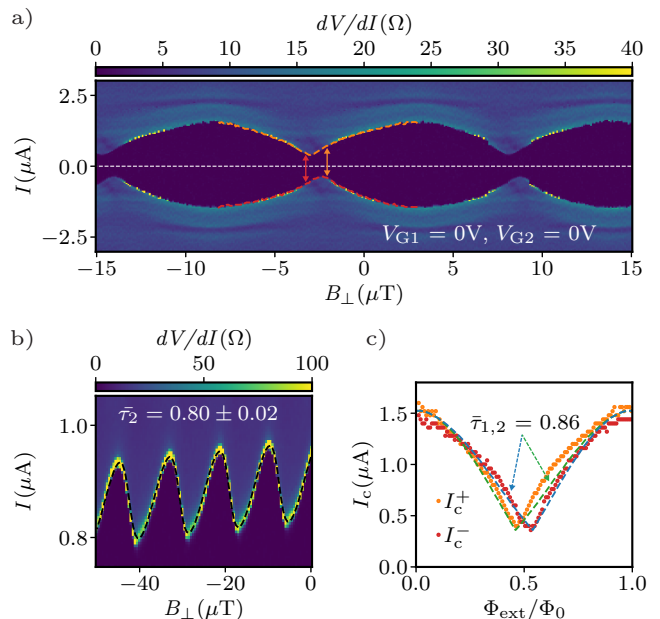


Figure 2. a) SQUID oscillations with  $V_{G1} = V_{G2} = 0$ . The critical currents  $I_c^+$  and  $I_c^-$  over one flux period are highlighted in orange and red respectively. At fixed magnetic field, the absolute value of the critical current in the two sweep directions is not the same. This is best seen in the region  $-5 < B_\perp < 0 \mu\text{T}$  with a visible example taken at the red and orange arrows, where the diode effect has a magnitude of  $\sim 23\%$ . b) Measurement for a strongly asymmetric SQUID setting with  $V_{G1} = 0$  V and  $V_{G2} = -1.1$  V. Here, the junction with the large critical current JJ<sub>1</sub> serves as the reference junction. As a consequence, the critical current as a function of flux now reflects the CPR of the weaker junction JJ<sub>2</sub>. The CPR is strongly non-sinusoidal and a fit (black dashed line) yields  $\bar{\tau}_2 = 0.8$ . c) Plot of the extracted  $I_c^+$  (orange) and  $I_c^-$  (red) taken from the measurement shown in a). The dashed two curves (green and blue) show simplified model fits with  $\bar{\tau}_{1,2} = 0.86$  and the critical currents of the junctions taken from Fig. 1c)

As introduced before, a contribution from loop inductances may generate the diode effect, too, if the loop inductances in the two arms are different. Applying finite element simulations, we obtain  $L_1 \approx 39$  pH and  $L_2 \approx 44$  pH. First, we note that the relative phase shifts between the two arms is small,  $< 10 \text{ pH} \times 1 \mu\text{A} \times 2\pi / \Phi_0 = 0.03$  rad. Hence, we only expect a small diode effect due to loop inductances. We properly simulate the effect of the loop inductances on the critical current of the SQUID in the SM and find that the loop inductances alone cannot explain the observed diode effect in our experiment.

We also note that the measured CPR of the SQUID in Fig. 2a) is periodic with a periodicity of  $11.6 \mu\text{T}$ . Since this should correspond to an added flux quantum  $\Phi_0$  in the loop area  $A_l$ , we obtain for  $A_l = 177 \mu\text{m}^2$ . This is approximately a factor three bigger than the geometrical area defined by the etched square-shaped hole of size  $7.2 \times 7.4 = 53 \mu\text{m}^2$ . It is known that the screening given by



the London penetration length  $\lambda_L$  gets much enlarged in very thin superconducting films of thickness  $t$ . It is actually given by the Pearl length [58] which, in the limit of films much tinner than the bulk  $\lambda_L$ , is given by  $\lambda_L^2/t$ . Using this equation we obtain for the London screening length  $\lambda_D \approx 170$  nm, which if compared with literature values for Al is still large. Typical literature values are  $\lambda_D \approx 50$  nm. [59] This discrepancy indicates that the magnetic-field in this geometry is not very well screened.

Fig. 2b) shows a measurement of the CPR of a single junction, obtained during the same cool-down. Here,  $V_{G1} = 0$  V and  $V_{G2} = -1.1$  V so that the current in  $JJ_1$  is large  $\sim 0.9$   $\mu$ A and in  $JJ_2$  it is small  $\sim 0.1$   $\mu$ A. In such a situation  $JJ_1$  acts as reference junction and the critical current of the weak junction  $JJ_2$  can be obtained from Eq. 5 as

$$I_c^+ = \max_{\varphi} (I_1(\varphi) + I_2(\varphi - \varphi_{\text{ext}})) \quad (6)$$

$$I_c^+(\varphi_{\text{ext}}) \simeq I_{c1} + I_2(\varphi_1^* - \varphi_{\text{ext}}), \quad (7)$$

where  $\varphi_1^*$  is the phase value for which  $JJ_1$  has its maximal value  $I_{c1}$ . Hence, we see that under the condition that the reference junction dominates, we obtain the dependence of the critical current of the weak junction as a function of phase. Applying Eq. 2 to fit the measured data yields for the effective transmission probability  $\bar{\tau} = 0.8 \pm 0.02$ . This is a large value, showing that the CPR is strongly non-sinusoidal, something that is visibly seen in the graph of Fig. 2b). If one makes use of the universal bimodal distribution function of transmission eigenvalues to determine the effective  $\bar{\tau}$  [47, 53–55], one obtains  $\bar{\tau} = 0.866$ . Including different devices nominally fabricated the same way, we always find a large effective transmission value of order  $\sim 0.8$  in agreement with theoretical expectations.

In Fig. 2c) we compare the critical currents extracted from Fig. 2a) with the simplified model of Eq. 5. We take the measured critical currents of the two junctions as input parameters, i.e.  $I_{c1} = 0.87$   $\mu$ A and  $I_{c2} = 0.67$   $\mu$ A, and assume  $\bar{\tau}_1 = \bar{\tau}_2 = \bar{\tau}$  as a single fitting parameter. The best agreement is obtained for  $\bar{\tau} = 0.86$ . We note, that a similar model calculation based only on loop inductances barely matches the measurement. It is shown as a comparison in the SM.

The fits for  $I_c^+$  (green) and  $I_c^-$  (blue) reproduce the relative shift along the flux axis very well. The shape of the curves is, however, not reproduced so well. In the region  $\Phi_{\text{ext}}/\Phi_0 \in [0.25, 0.5]$  and  $\Phi_{\text{ext}}/\Phi_0 \in [0.5, 0.75]$  respectively, the measured  $I_c^+$  and  $I_c^-$  curves are higher than what is obtained with the model. Deviations between the experimental and the modelled curves could be attributed to the choice of CPR used in the model. First, we considered an average transparency instead of a distribution of transparencies. Second, the expression of the current carried by the Andreev bound states could be different from Eq. 2, since our junctions could be in a regime intermediate to the short and long junction limit. And, in the third place, spin-orbit effects may affect the

Table I. Conditions for obtaining a diode effect (DE). An extended table that includes the loop inductances can be found in the SM. The first column is used to distinguish the classical sinusoidal CPR ( $\bar{\tau} = 0$ ) from a strongly skewed CPR described by a highly transmissive ballistic JJ with a mean transmission probability  $\bar{\tau} > 0$ .  $\alpha$  ( $\beta$ ) denotes the asymmetry in critical currents (transmission probabilities) of the two junctions.

$\bar{\tau}$	$\alpha$	$\beta$	DE
0	0	n.a.	no
0	$\neq 0$	n.a.	no
$\neq 0$	0	0	no
$\neq 0$	0	$\neq 0$	yes
$\neq 0$	$\neq 0$	0	yes
$\neq 0$	$\neq 0$	$\neq 0$	yes

CPR, too. For junctions of similar length in the same material system, it has been shown that spin-orbit interaction splits the ABS into spinful states with different dispersion relations [60]. Noticeably, the experiment indicates that these deviations result in an increase of the diode effect compared to what is predicted by the simple model.

Having established that a diode effect appears in a SQUID with junctions having a non-sinusoidal CPR with asymmetry, we summarize in Table III the necessary conditions for the diode effect (DE). To describe the asymmetry we introduce two asymmetry parameters  $\alpha$  and  $\beta$  for the critical currents and the transmission probabilities, respectively:

$$\alpha = \frac{I_{c1} - I_{c2}}{I_{c1} + I_{c2}} \quad \text{and} \quad \beta = \frac{\bar{\tau}_1 - \bar{\tau}_2}{\bar{\tau}_1 + \bar{\tau}_2} \quad (8)$$

This table can be extended taking the loop inductance into account. This is introduced in the SM with the additional parameters  $\varphi_L = 4\pi\bar{I}_c L/\Phi_0$ , where  $L$  is the loop inductance,  $\bar{I}_c$  the mean critical current of the two junctions, and additionally the loop inductance asymmetry defined as  $\gamma = (L_1 - L_2)/(L_1 + L_2)$  with  $L_1$  and  $L_2$  the inductances in the two arms, respectively. This extended table has 18 non-trivial entries and clearly shows that the diode effect appears when the SQUID arm is asymmetric with the only exception for the situation with two sinusoidal CPRs. Here, an asymmetry in the critical current  $I_{c1} \neq I_{c2}$  is not sufficient to generate the diode effect.

#### IV. GATE TUNABLE DIODE EFFICIENCY

The diode effect can be quantified via the diode efficiency, defined as

$$\eta = \frac{I_c^+ - I_c^-}{I_c^+ + I_c^-}. \quad (9)$$

In Fig. 3, we show the diode efficiency  $\eta$  as a function of external flux  $\Phi_{\text{ext}}/\Phi_0$  for different gate configurations as obtained from the experiment (left) and as calculated from the model (right). In the model, we make use of the relation between critical current and gate voltage of the individual junctions  $I_{c_i}(V_{G_i})$  and use these values as input parameters in the first approximation. We also use the simulated loop inductance values from which we obtain the phase response due to screening  $\varphi_L$  and the loop inductance asymmetry  $\gamma$ . We assume that the effect of the gate voltage is mainly to change the critical current value  $I_{c_i}$  through the number of channels  $N$ , while  $\bar{\tau}_i$  roughly stays constant. We fix  $\bar{\tau}_1 = \bar{\tau}_2 = 0.86$ , but we note that the calculated  $\eta$  plot is insensitive if one varies  $\bar{\tau}_2$  between 0.8 and 0.9.

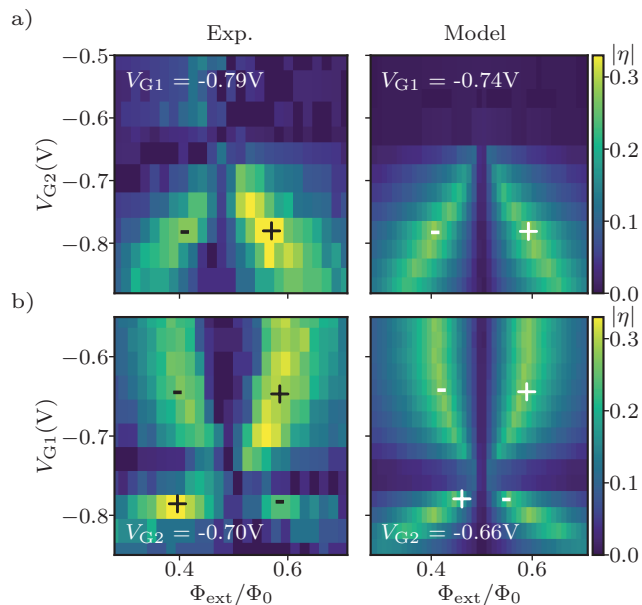


Figure 3. Magnitude of the diode efficiency  $|\eta|$  as a function of external flux  $\Phi_{\text{ext}}$  for different gate configurations as obtained from the measurements (left) and as calculated from the model (right). The sign of  $\eta$  is indicated on the visible lobes with + and -. The model takes into account the numerically simulated loop inductances, their asymmetry, and the values  $I_{c(1,2)}$  of the two junctions obtained from the measurements in Fig. 1c). The JJ transparencies were fixed to  $\bar{\tau}_1 = \bar{\tau}_2 = 0.86$ . (a)  $|\eta|$  as a function of  $V_{G2}$  at fixed  $V_{G1}$ , and (b)  $|\eta|$  as a function of  $V_{G1}$  at fixed  $V_{G2}$ . Note, that for  $\varphi_{\text{ext}} = 0.5$ ,  $\eta = 0$  independent on any other parameters.

In Fig. 3a), we plot  $|\eta|$  for different values of  $V_{G2}$  at fixed  $V_{G1}$ . Both in the experiment and in the model,  $|\eta|$  drops for  $-0.7 < V_{G2} < -0.5$  V. As seen in Fig. 1c), this corresponds to a gate configuration with  $I_{c1} \approx I_{c2}$ , so that  $\alpha \approx 0$ . As expected, the absence of critical current asymmetry lowers the diode efficiency. To obtain in the model the same diode efficiencies  $\eta$  as measured, we had to increase the critical current of JJ<sub>1</sub>. In the experiment, we had  $V_{G1}$  fixed at  $-0.79$  V, which would correspond

to  $I_{c1} = 470$  nA. However, in order to match the model with the data, we had to use 710 nA, corresponding to  $V_{G1} = -0.74$  V, as indicated in the top left corner of the figure. Without this correction, the measured  $\eta$  values would have been larger than what the model predicts. We attribute this difference in gate voltage to gate-jumps that occur from time-to-time. We emphasize, that between the measurements for Fig. 1c) and the ones for Fig. 2a) lie days.

In the same manner as before we present in Fig. 3b) the efficiencies, now reversed for different values of  $V_{G1}$  at fixed  $V_{G2} = -0.7$  V. As before, to match the model to the experiment, we had to increase  $I_{c2}$  from the initially measured value of 590 nA at  $V_{G2}$  to 650 nA, which correspond to  $I_{c2}$  measured at  $V_{G2} = -0.66$  V.

Both in the experiment and in the model one can observe the typical butterfly pattern of  $\eta$  as predicted in Ref. [1]. The two arms of maximum  $|\eta|$  meet in the point of minimum asymmetry at  $\Phi_{\text{ext}}/\Phi_0 = 0.5$  for  $V_{G2} \approx -0.65$  V and  $V_{G1} \approx -0.75$  V for a) and b) respectively, where  $\eta$  drops to 0.

The model qualitatively reproduce the gate dependence of the diode efficiency very well. We obtain a maximum  $|\eta|$  of  $\simeq 0.3$  from the experiment. This 30% efficiency is much larger than what has previously been obtained in a SQUID with asymmetric loop inductance [61]. Taking a SQUID model with a single channel JJ junction, we numerically find for the maximum efficiency  $\eta = 0.37$ . This is obtained for  $\tau_1 = 1$  and  $\tau_2 = 0.75$  or the reversed. This could be achieved by combining a single channel ballistic  $\tau = 1$  Josephson junction realized in atomic contacts [44] with a semiconductor-superconductor hybrid devices as we have discussed here.

## V. CONCLUSION

In conclusion, we have investigated the origin of the Josephson diode effect in a supercurrent interferometer. We show that in our system the diode effect is due to the non-sinusoidal character of the JJs and hence due to a subtle interference between higher-order harmonics of the CPRs of the individual JJs. In addition to higher harmonics, an asymmetry either in the composition of the Fourier components in the CPR or in the critical current of the two JJ is required to obtain a diode effect. Future directions include the possibility to concatenate more SQUIDS in parallel in order to further increase the diode efficiency as was proposed in Ref. [1].

## ACKNOWLEDGMENTS

We thank C. M. Marcus for his support in initiating this work and collaboration. This research was supported by the Swiss Nanoscience Institute (SNI), the Swiss National Science Foundation through grants No 172638 and 192027, and the QuantEra project SuperTop. We further acknowledge funding from the European Union's

Horizon 2020 research and innovation programme, specifically a) from the European Research Council (ERC) grant agreement No 787414, ERC-Adv TopSupra, b) grant agreement No 828948, FET-open project AndQC, c) grant agreement 847471, project COFUND-QUSTEC,

and d) grant agreement 862046, project TOPSQUAD. Constantin Schrade acknowledges support from the Microsoft Corporation. All data in this publication is available in numerical form at: <https://doi.org/10.5281/zenodo.7733057>.

- 
- [1] R. S. Souto, M. Leijnse, and C. Schrade, Josephson diode effect in supercurrent interferometers, *Physical Review Letters* **129**, 267702 (2022).
- [2] B. Josephson, Possible new effects in superconductive tunnelling, *Physics Letters* **1**, 251 (1962).
- [3] A. A. Golubov, M. Y. Kupriyanov, and E. Il'ichev, The current-phase relation in josephson junctions, *Reviews of Modern Physics* **76**, 411 (2004).
- [4] M. R. Buitelaar, T. Nussbaumer, and C. Schönenberger, Quantum dot in the kondo regime coupled to superconductors, *Physical Review Letters* **89**, 256801 (2002).
- [5] M. S. Choi, M. Lee, K. Kang, and W. Belzig, Kondo effect and josephson current through a quantum dot between two superconductors, *Physical Review B* **70**, 020502(R) (2004).
- [6] R. Maurand, T. Meng, E. Bonet, S. Florens, L. Marty, and W. Wernsdorfer, First-order 0- $\pi$  quantum phase transition in the kondo regime of a superconducting carbon-nanotube quantum dot], *Physical Review X* **2**, 011009 (2012).
- [7] A. I. Buzdin, L. N. Bulaevskii, and S. V. Panyukov, Critical-current oscillations as a function of the exchange field and thickness of the ferromagnetic metal (f) in an s-f-s josephson junction, *JETP Letters* **35**, 178 (1982).
- [8] A. Buzdin,  $\pi$ -junction realization due to tunneling through a thin ferromagnetic layer, *JEPT Letters* **78**, 583 (2003).
- [9] V. V. Ryazanov, V. A. Oboznov, A. Y. Rusanov, A. V. Veretennikov, A. A. Golubov, and J. Aarts, Coupling of two superconductors through a ferromagnet: Evidence for a  $\pi$  junction, *Physical Review Letters* **86**, 2427 (2001).
- [10] T. Kontos, M. Aprili, J. Lesueur, F. Genêt, B. Stephanidis, and R. Boursier, Josephson junction through a thin ferromagnetic layer: Negative coupling, *Physical Review Letters* **89**, 137007 (2002).
- [11] E. C. Gingrich, B. M. Niedzielski, J. A. Glick, Y. Wang, D. L. Miller, R. Loloee, W. P. P. Jr, and N. O. Birge, Controllable  $\pi$  josephson junctions containing a ferromagnetic spin valve, *Nature Physics* **12**, 564 (2016).
- [12] H. Sickinger, A. Lipman, M. Weides, R. G. Mints, H. Kohlstedt, D. Koelle, R. Kleiner, and E. Goldobin, Experimental evidence of a  $\phi$  josephson junction, *Physical Review Letters* **109**, 107002 (2012).
- [13] I. V. Krive, L. Y. Gorelik, R. I. Shekhter, and M. Jonson, Chiral symmetry breaking and the josephson current in a ballistic superconductor-quantum wire-superconductor junction, *Low Temperature Physics* **30**, 398 (2004).
- [14] A. A. Reynoso, G. Usaj, C. A. Balseiro, D. Feinberg, and M. Avignon, Anomalous josephson current in junctions with spin polarizing quantum point contacts, *Physical Review Letters* **101**, 107001 (2008).
- [15] A. Zazunov, R. Egger, T. Jonckheere, and T. Martin, Anomalous josephson current through a spin-orbit coupled quantum dot, *Physical Review Letters* **103**, 147004 (2009).
- [16] T. Yokoyama, M. Eto, and Y. V. Nazarov, Josephson current through semiconductor nanowire with spin-orbit interaction in magnetic field, *Journal of the Physical Society of Japan* **82**, 054703 (2013).
- [17] D. B. Szombati, S. Nadj-Perge, D. Car, S. R. Plissard, E. P. A. M. Bakkers, and L. P. Kouwenhoven, Josephson  $\phi_0$ -junction in nanowire quantum dots, *Nature Physics* **12**, 568 (2016).
- [18] C. B. L., Fuchs, A. Costa, J. J. Pico-Cortes, S. Reinhardt, S. Gronin, G. C. Gardner, T. Lindemann, M. J. Manfra, P. E. F. Junior, D. Kochan, J. J. Fabian, N. Paradiso, and C. Strunk, Effect of rashba and dresselhaus spin-orbit coupling on supercurrent rectification and magnetochiral anisotropy of ballistic josephson junctions, *Journal of Physics-Condensed Matter* **34**, 10.1088/1361-648X/ac4d5e (2022).
- [19] A. Buzdin, Direct coupling between magnetism and superconducting current in the josephson  $\phi_0$  junction, *Physical Review Letters* **101**, 107005 (2008).
- [20] R. Wakatsuki, Y. Saito, S. Hoshino, Y. M. Itahashi, T. Ideue, M. Ezawa, Y. Iwasa, and N. Nagaosa, Nonreciprocal charge transport in noncentrosymmetric superconductors, *Science Advances* **3**, 10.1126/sciadv.1602390 (2017).
- [21] G. L. J. A. Rikken, J. Fölling, and P. Wyder, Electrical magnetochiral anisotropy, *Physical Review Letters* **87**, 236602 (2001).
- [22] G. L. J. A. Rikken and P. Wyder, Magnetoelectric anisotropy in diffusive transport, *Physical Review Letters* **94**, 016601 (2005).
- [23] F. Ando, Y. Miyasaka, T. Li, J. Ishizuka, T. Arakawa, Y. Shiota, T. Moriyama, Y. Yanase, and T. Ono, Observation of superconducting diode effect, *Nature* **584**, 373 (2020).
- [24] A. Daido, Y. Ikeda, and Y. Yanase, Intrinsic superconducting diode effect, *Physical Review Letters* **128**, 037001 (2022).
- [25] C. Baumgartner, L. Fuchs, A. Costa, S. Reinhardt, S. Gronin, G. C. Gardner, T. Lindemann, M. J. Manfra, P. F. F. Junior, D. Kochan, J. Fabian, N. Paradiso, and C. Strunk, Supercurrent rectification and magnetochiral effects in symmetric josephson junctions, *Nature Nanotechnology* **17**, 39 (2022).
- [26] L. Bauriedl, C. Bäuml, L. Fuchs, C. Baumgartner, N. Paulik, J. M. Bauer, K.-Q. Lin, J. M. Lupton, T. Taniguchi, K. Watanabe, C. Strunk, and N. Paradiso, Supercurrent diode effect and magnetochiral anisotropy in few-layer nbse<sub>2</sub>, *Nature Communications* **13**, 10.1038/s41467-022-31954-5 (2022).
- [27] H. Wu, Y. Wang, Y. Xu, P. K. Sivakumar, C. Pasco, U. Filippozzi, S. S. P. Parkin, Y.-J. Zeng, T. McQueen, and M. N. Ali, The field-free josephson diode in a van der waals heterostructure, *Nature* **604**, 653 (2022).

- [28] J.-X. Lin, P. Siriviboon, H. D. Scammell, S. Liu, D. Rhodes, K. Watanabe, T. Taniguchi, J. Hone, M. S. Scheurer, and J. I. A. Li, Zero-field superconducting diode effect in small-twist-angle trilayer graphene, *Nature Physics* **18**, 1221 (2022).
- [29] N. F. Q. Yuan and L. Fu, Supercurrent diode effect and finite-momentum superconductors, *Proceedings of the National Academy of Sciences of the United States of America* **119**, 10.1073/pnas.2119548119 (2022).
- [30] M. Davydova, S. Prembabu, and L. Fu, Universal josephson diode effect, *Science Advances* **8**, 10.1126/sciadv.abo0309 (2022).
- [31] B. Pal, A. Chakraborty, P. K. Sivakumar, M. Davydova, A. K. Gopi, A. K. Pandeya, J. A. Krieger, Y. Zhang, M. Date, S. Ju, N. Yuan, N. B. M. S. L. Fu, and S. S. P. Parkin, Josephson diode effect from cooper pair momentum in a topological semimetal, *Nature Physics* **18**, 1228 (2022).
- [32] C.-Z. Chen, J. J. He, M. N. Ali, G.-H. Lee, K. C. Fong, and K. T. Law, Asymmetric josephson effect in inversion symmetry breaking topological materials, *Physical Review B* **98**, 075430 (2018).
- [33] A. Kononov, G. Abulizi, K. Qu, J. Yan, D. Mandrus, K. Watanabe, T. Taniguchi, and C. Schönberger, One-dimensional edge transport in few-layer  $\text{wTe}_2$ , *Nano Letters* **20**, 4228 (2020).
- [34] H. F. Legg, D. Loss, and J. Klinovaja, Superconducting diode effect due to magnetochiral anisotropy in topological insulators and rashba nanowires, *Physical Review B* **106**, 104501 (2022).
- [35] T. A. Fulton and R. C. Dynes, Current-phase relations in superconducting bridges, *Physical Review Letters* **25**, 794 (1970).
- [36] T. A. Fulton, L. N. Dunkleberger, and R. C. Dynes, Quantum interference properties of double josephson junctions, *Physical Review B* **6**, 855 (1972).
- [37] W.-T. Tsang and T. V. Duzer, dc analysis of parallel arrays of two and three josephson junctions, *Journal of Applied Physics* **46**, 4573 (1975).
- [38] A. Barone and G. Paterno, *Physics and Applications of the Josephson Effect* (John Wiley & Sons, New York, 1982).
- [39] Y.-J. Doh, J. A. van Dam, A. L. Roest, E. P. A. M. Bakkers, L. P. Kouwenhoven, and S. D. Franceschi, Tunable supercurrent through semiconductor nanowires, *Science* **309**, 272 (2005).
- [40] T. W. Larsen, K. D. Petersson, F. Kuemmeth, T. S. Jespersen, P. Krogstrup, J. Nygård, and C. M. Marcus, Semiconductor-nanowire-based superconducting qubit, *Physical Review Letters* **115**, 127001 (2015).
- [41] E. Prada, P. San-Jose, M. W. A. de Moor, A. Geresdi, E. J. H. Lee, J. Klinovaja, D. Loss, J. Nygård, R. Aguado, and L. P. Kouwenhoven, From andreev to majorana bound states in hybrid superconductor-semiconductor nanowires, *Nature Reviews Physics* **2**, 575 (2020).
- [42] G. Burkard, M. J. Gullans, X. Mi, and J. R. Petta, Superconductor-semiconductor hybrid-circuit quantum electrodynamics, *Nature Reviews Physics* **2**, 129 (2020).
- [43] M. C. Koops, G. V. van Duyneveldt, and R. de Bruyn Ouboter, Direct observation of the current-phase relation of an adjustable superconducting point contact, *Physical Review Letters* **77**, 2542 (1996).
- [44] M. L. DellaRocca, M. Chauvin, B. Huard, H. Pothier, D. Esteve, and C. Urbina, Measurement of the current-phase relation of superconducting atomic contacts, *Physical Review Letters* **99**, 127005 (2007).
- [45] J. S. Lee, B. Shojaei, M. Pendharkar, A. P. McFadden, Y. Kim, H. J. Suominen, M. Kjaergaard, F. Nichele, H. Zhang, C. M. Marcus, and C. J. Palmström, Transport studies of epi-al/inas two-dimensional electron gas systems for required building-blocks in topological superconductor networks, *Nano Letters* **19**, 3083 (2019).
- [46] F. Nichele, E. Portolés, A. Fornieri, A. M. Whiticar, A. C. C. Drachmann, S. Gronin, T. Wang, G. C. Gardner, C. Thomas, A. T. Hatke, M. J. Manfra, and C. M. Marcus, Relating andreev bound states and supercurrents in hybrid josephson junctions, *Physical Review Letters* **124**, 226801 (2020).
- [47] O. Dorokhov, On the coexistence of localized and extended electronic states in the metallic phase, *Solid State Communications* **51**, 381 (1984).
- [48] G. Nanda, J. L. Aguilera-Servin, P. Rakyta, A. Kormányos, R. Kleiner, D. Koelle, K. Watanabe, T. Taniguchi, L. M. K. Vandersypen, and S. Goswami, Current-phase relation of ballistic graphene josephson junctions, *Nano Letters* **17**, 3396 (2017).
- [49] L. Bretheau, J. I.-J. Wang, R. Pisoni, K. Watanabe, T. Taniguchi, and P. Jarillo-Herrero, Tunnelling spectroscopy of andreev states in graphene, *Nature Physics* **13**, 756 (2017).
- [50] D. A. Manjarrés, S. GómezPáez, and W. J. Herrera, Skewness and critical current behavior in a graphene josephson junction, *Physical Review B* **101**, 064503 (2020).
- [51] D. I. Indolese, P. Karnatak, A. Kononov, R. Delagrè, R. Haller, L. Wang, P. Makk, K. Watanabe, T. Taniguchi, and C. Schönberger, Compact squid realized in a double-layer graphene heterostructure, *Nano Letters* **20**, 7129 (2020).
- [52] R. Haller, G. Fülöp, D. Indolese, J. Ridderbos, R. Kraft, L. Y. Cheung, J. H. Ungerer, K. Watanabe, T. Taniguchi, D. Beckmann, R. Danneau, P. Virtanen, and C. Schönberger, Phase-dependent microwave response of a graphene josephson junction, *Physical Review Research* **4**, 013198 (2022).
- [53] I. O. Kulik and A. N. Omel'yanchuk, Contribution to the microscopic theory of the josephson effect in superconducting bridges, *JETP Letters* **21**, 216 (1975).
- [54] Y. V. Nazarov, Limits of universality in disordered conductors, *Physical Review Letters* **73**, 134 (1994).
- [55] C. W. J. Beenakker, Random-matrix theory of quantum transport, *Reviews of Modern Physics* **69**, 731 (1997).
- [56] C. D. Tesche and J. Clarke, dc SQUID: Noise and optimization, *Journal of Low Temperature Physics* **29**, 301 (1977).
- [57] J. Clarke and A. I. Braginski, eds., *The SQUID Handbook, Fundamentals and Technology of SQUIDS and SQUID Systems, Vol. I* (WILEY-VCH Verlag GmbH, Weinheim, Germany, 2004).
- [58] A. I. Gubin, K. S. Ilin, S. A. Vitusevich, M. Siegel, N., and Klein, Dependence of magnetic penetration depth on the thickness of superconducting nb thin films, *Physical Review B* **72**, 064503 (2005).
- [59] T. Faber, A. B. Pippard, and D. Shoenberg, The penetration depth and high-frequency resistance of superconducting aluminium, *Proceedings of the Royal Society of London. Series A. Mathematical and Physical Sciences* **231**, 336 (1955).



- [60] L. Tosi, C. Metzger, M. F. Goffman, C. Urbina, H. Pothier, S. Park, A. L. Yeyati, J. Nygard, and P. Krogstrup, Spin-orbit splitting of andreev states revealed by microwave spectroscopy, [Physical Review X](#) **9**, 011010 (2019).
- [61] F. Paolucci, G. D. Simoni, and F. Giazotto, A gate- and flux-controlled supercurrent diode effect, [Applied Physics Letters](#) **122**, 042601 (2023).
- [62] D. C. Mattis and J. Bardeen, Theory of the anomalous skin effect in normal and superconducting metals, [Physical Review](#) **111**, 412 (1958).
- [63] M. Tinkham, [Introduction to Superconductivity](#), 2nd ed. (Dover Publications, 2004).
- [64] A. J. Annunziata, D. F. Santavicca, L. Frunzio, G. Catelani, M. J. Rooks, A. Frydman, and D. E. Prober, Tunable superconducting nanoinductors, [Nanotechnology](#) **21**, 10.1088/0957-4484/21/44/445202 (2010).

## Supplemental Material: Gate Tunable Josephson Diode in Proximitized InAs Supercurrent Interferometers

### SI. FABRICATION & MEASUREMENT SET-UP

The wafer used in this experiment was grown by molecular beam epitaxy (MBE). The stack consists of an InP substrate, a 1- $\mu\text{m}$ -thick buffer realized with  $\text{In}_{1-x}\text{Al}_x\text{As}$  alloys, a 4 nm  $\text{In}_{0.75}\text{Ga}_{0.25}\text{As}$  bottom barrier, a 7 nm InAs layer, a 10 nm  $\text{In}_{0.75}\text{Ga}_{0.25}\text{As}$  top barrier, two monolayers of GaAs acting as stop etch layer, and 10 nm of Al deposited *in situ* without breaking the MBE vacuum. The two-dimensional electron gas is characterized from Hall bar devices and shows electron mobility peak of  $\mu = 12\,000\text{ cm}^2\text{V}^{-1}\text{s}^{-1}$  for an electron density of  $16 \times 10^{11}\text{ cm}^{-2}$ , corresponding to an electron mean free path of  $l_e \approx 230\text{ nm}$ .

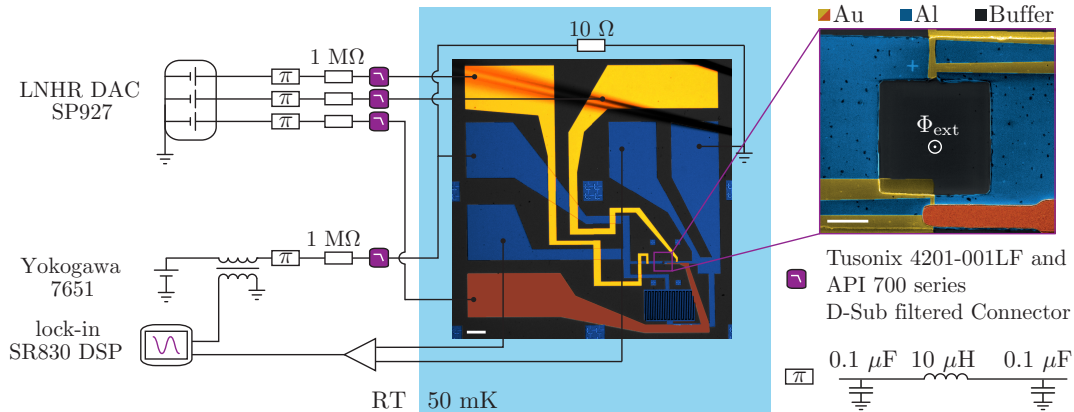


Figure S1. a) False color optical image of the full device together with a sketch of the measurement setup. The scale bar is 100  $\mu\text{m}$ . b) Zoom-in over the SQUID showing the loop area threaded by the external flux  $\Phi_{\text{ext}}$ . The electron density in the junction region is tuned via a set of gates coloured in yellow and orange. The scale bar is 3  $\mu\text{m}$

The device is fabricated using standard electron beam lithography techniques. The MESA is electrically isolated by first removing the top Al film with Al etchant Transene D, followed by a deep III-V chemical wet etch  $\text{H}_2\text{O}:\text{C}_6\text{H}_8\text{O}_7:\text{H}_3\text{PO}_4:\text{H}_2\text{O}_2$  (220:55:3:3). Next, the Al film on the mesa is selectively etched with Al etchant Transene D to define the planar JJ. Electrostatic gates are made of two Ti/Au layers, isolated from the Al and from each other by hafnium oxide ( $\text{HfO}_2$ ) layers grown by atomic layer deposition (ALD) at a temperature of 90  $^\circ\text{C}$  over the entire sample. The first layer of gates is made of electron-beam evaporated Ti/Au (5 nm/25 nm) on top of 15 nm of  $\text{HfO}_2$ . Connections to the external circuit are obtained by evaporating Ti/Au (5/85 nm) leads at  $\pm 17^\circ$  to overcome the MESA step. A second layer of gates, made of angle-evaporated Ti/Au (5/85 nm), is patterned on top of 25 nm of  $\text{HfO}_2$ .

Measurements are carried out in a Triton 200 cryogen-free dilution refrigerator with a base temperature of  $\approx 50\text{ mK}$ . A detailed overview of the measurement set-up is shown in Fig.S1. Our setup sources a current using a 1 M $\Omega$  resistor in series to a dc voltage source on which a small ac component with frequency  $f = 17.7\text{ Hz}$ , supplied by a lock-in amplifier, is superposed. This current is applied to the source contact of the SQUID on the left with the drain contact on the right side galvanically connected to ground. The SQUID is shunted at the source to ground with a resistor  $R_S = 10\ \Omega$ . This shunt resistor is directly placed on the sample holder. In addition, a finger capacitance of  $\approx 0.7\text{ pF}$  is patterned in parallel to the SQUID (lower right of the optical image). The original purpose of the capacitance was to increase the quality factor of the Josephson junctions. However, its effect is negligible, since the capacitance provided by the leads is larger. We measure the differential resistance of the shunted device using a voltage amplifier and lock-in techniques. The flux through the SQUID is generated by a vector magnet.

## SII. ESTIMATION OF LOOP INDUCTANCE

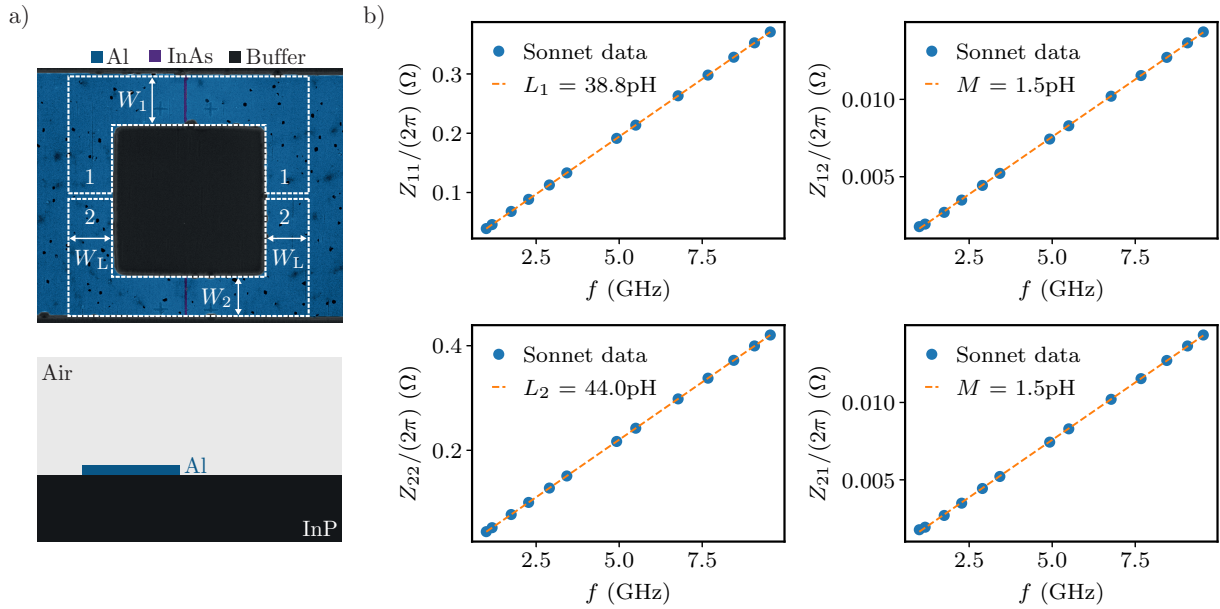


Figure S2. Sonnet simulations of the loop inductances. The superconducting loop is segmented into an upper (lower) branch 1 (2) with width  $W_1 = 3 \mu\text{m}$  ( $W_2 = 2.5 \mu\text{m}$ ). The two inductances  $L_1$ ,  $L_2$  and the mutual inductance  $M$  are deduced from the slope of the frequency dependent impedances. We see that  $M \ll L_{1,2}$  and that there is an asymmetry of  $\sim 6 \%$  in the loop inductances.

In the following we will detail the evaluation of the inductance of the loop branches. The loop geometry is defined as indicated by the white dashed lines in Fig.S2a). The width of the two branches corresponds to the junctions width in the upper and lower path ( $W_1 = 3 \mu\text{m}$ ,  $W_2 = 2.75 \mu\text{m}$ ) and it is set equal to  $W_L = (W_1 + W_2)/2 = 2.75 \mu\text{m}$  laterally. Note that the inductance calculated for this geometry will be an upper bound to the inductance of the device, being the leads wider on the left and right side of the loop. With finite-element simulations performed in Sonnet, we compute the two-port impedance for different frequencies. The impedance is evaluated between two sets of floating co-calibrated ports, positioned on each side of the loop. In the simulation we use InP as a substrate, with a relative dielectric constant  $\epsilon_r = 12.4$ . The kinetic inductance of the Al film is evaluated by measuring the temperature dependence of the resistance of an Al bar realized on a different chip from the same wafer. We measure a critical temperature of 1.25K and a normal state resistance of 15.5  $\Omega$ . Using the low frequency limit of the Mattis-Bardeen screening theory [S62–S64], one obtains for the kinetic sheet inductance:

$$L_{\text{kin}/\square} = \frac{\hbar R_{\text{n}/\square}}{\pi \Delta_0} \tanh^{-1} \left( \frac{\Delta_0}{2k_B T} \right). \quad (\text{S1})$$

Here,  $R_{\text{n}/\square}$  is the normal state sheet resistance,  $\Delta_0$  the zero-temperature BCS gap and  $T$  the absolute temperature. Using Eq. S1 we extract  $L_{\text{kin}/\square} \approx 5\text{nH}$ .

### SIII. RETRAPPING VERSUS SWITCHING CURRENT

In Fig. S3 we compare the switching current with the retrapping current values. We show that the two values coincide in this experiment. We think that is due to the low parallel resistor which keeps the voltage over the junction small in the normal state, hence, reducing overheating effects. Additionally, the shunt resistor add damping at the plasma frequency of the junctions, which reduces the quality factor.

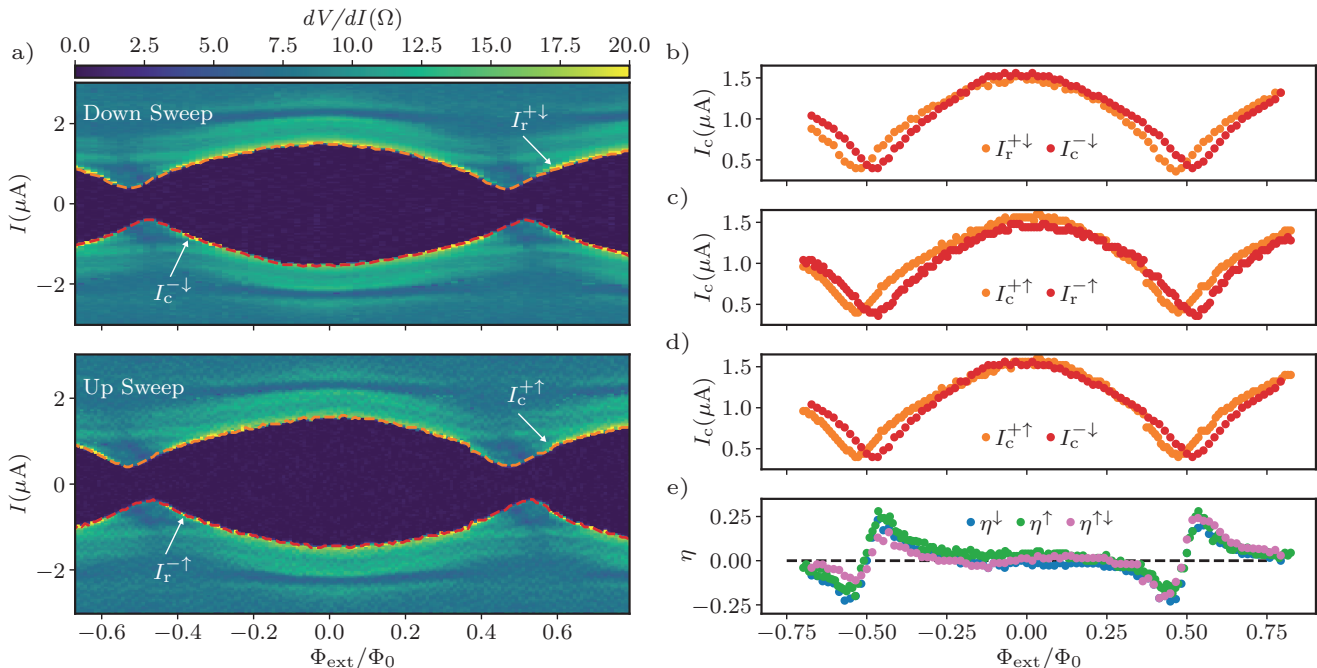


Figure S3. The two measurements in the first row were obtained for exact the same parameter settings, except for the direction of current-bias sweep. In the left (right) measurement the current was decreased (increased) starting with positive (negative) values at  $+3 \mu\text{A}$  ( $-3 \mu\text{A}$ ) and sweeping down (up) to  $-3 \mu\text{A}$  ( $+3 \mu\text{A}$ ). In the middle row, we show the current values for which the differential resistance shows a peak. This peak positions either correspond to the critical  $I_c$  or retrapping current  $I_r$ . On sweeping downwards, we denote the negative critical current as  $I_c^{-\downarrow}$  and the positive retrapping current as  $I_r^{+\downarrow}$ . In analogy, on sweeping upwards, the positive critical current is denoted by  $I_c^{+\uparrow}$  and the negative retrapping current by  $I_r^{-\uparrow}$ . In the left graph of the bottom row we compare the positive and negative critical currents, both obtained in a proper way using opposite sweep directions. Now we can compare the extracted diode efficiency for three cases: i) for the case when we extract the critical currents from sweeping the current bias into negative direction only,  $\eta^{\downarrow}$ , ii) into positive direction only,  $\eta^{\uparrow}$ , and iii), when we deduce the critical current properly,  $\eta^{\uparrow\downarrow}$ . All three methods yield qualitatively the same efficiencies with no significant differences. Importantly, one clearly cannot say that  $\eta^{\uparrow\downarrow}$  would yield in general lower efficiencies.



#### SIV. SQUID OSCILLATIONS AT DIFFERENT GATE VOLTAGES

Here, we show how the SQUID oscillations develop when the critical current of one junction is tuned from being larger, equal and finally smaller than the critical current of the other junction. Fig.S4 shows the differential resistance of the SQUID as a function of current bias and perpendicular magnetic field.  $V_{G2}$  is fixed at  $-0.5$  V, while  $V_{G1}$  is swept from  $-0.57$  V to  $-0.8$  V. As extracted from Fig.1c),  $I_{c2}(V_{G2} = -0.5$  V)  $\sim 720$  nA, while  $I_{c1}(V_{G1} = -0.57$  V)  $\sim 1.12$   $\mu$ A and  $I_{c1}(V_{G1} = -0.8$  V)  $\sim 360$  nA.

The sign of the diode efficiency is mirrored with respect the magnetic field value corresponding to half flux quantum when the critical current asymmetry  $\alpha$  between the two junctions changes sign. We also notice a dip in differential resistance developing around half flux quantum that evolves with  $\alpha$ .

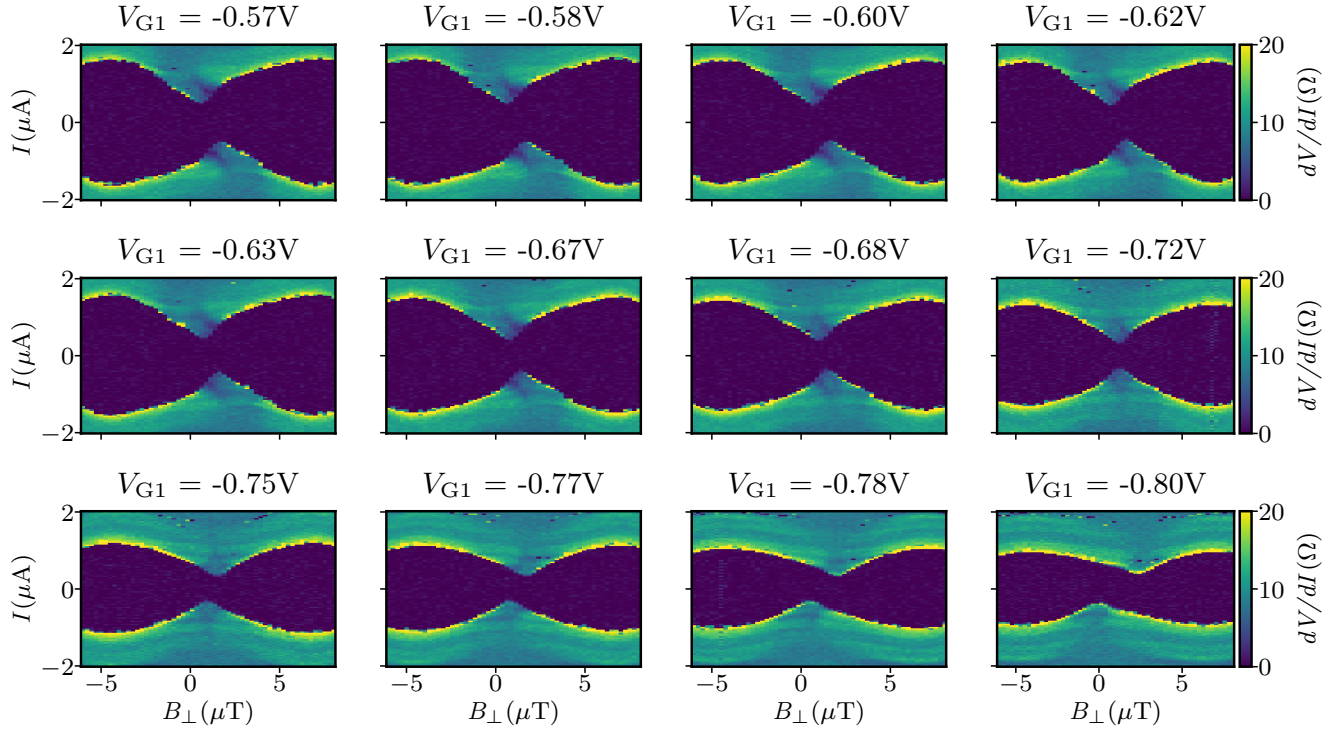


Figure S4. SQUID oscillation at different gate voltage configurations.  $V_{G2}$  is fixed at  $-0.5$  V, while  $V_{G1}$  is swept from  $-0.57$  V to  $-0.8$  V. The asymmetry in the SQUID oscillations follows the asymmetry in critical current between the two junctions. We have  $I_{c1}(V_{G1} = -0.57$  V)  $> I_{c2}(V_{G2} = -0.5$  V) and  $I_{c1}(V_{G1} = -0.8$  V)  $< I_{c2}(V_{G2} = -0.5$  V).

## SV. MODEL INCLUDING LOOP INDUCTANCES

We model the current-phase relation of a single junction  $i \in [1, 2]$  with

$$I_i(\varphi_1) = \frac{N_i \bar{\tau}_i e \Delta}{\hbar} \frac{\sin(\varphi_i)}{\sqrt{1 - \bar{\tau}_i \sin^2(\varphi_i/2)}}, \quad (\text{S2})$$

where  $N_i$  stands for the number of channels and  $\bar{\tau}_i$  for the mean transmission probability of junction  $i$ . We introduce the normalization parameter  $A_i$  as

$$A_i := \max_{\varphi_i} \left\{ \frac{\sin(\varphi_i)}{\sqrt{1 - \bar{\tau}_i \sin^2(\varphi_i)}} \right\}. \quad (\text{S3})$$

Note, that  $A_i$  only depends on  $\bar{\tau}_i$ . We thus get the normalized CPR as

$$I_i \varphi_1 = \frac{I_{ci}}{A_i} \frac{\sin(\varphi_i)}{\sqrt{1 - \bar{\tau}_i \sin^2(\varphi_i/2)}}. \quad (\text{S4})$$

In this notation of the CPR,  $N$  has been replaced by the critical current  $I_c$ , which appears now explicitly.

Flux quantization in the loop imposes:

$$\varphi_1 - \varphi_2 = 2\pi\Phi/\Phi_0. \quad (\text{S5})$$

Here, the total flux in the loop  $\Phi$  is given by the external flux  $\Phi_{\text{ext}}$  and the contributions from the screening currents expressed through the loop inductances,  $L_1$  and  $L_2$ , that belong to the two branches. If mutual inductances are considered, too, one has to introduce new effective inductances  $L'_1 = L_1 - M$  and  $L'_2 = L_2 - M$ , where  $M$  describes the mutual inductance. We obtain for the total flux:

$$\Phi = \Phi_{\text{ext}} - L'_1 I_1(\varphi_1) + L'_2 I_2(\varphi_2) \quad (\text{S6})$$

Therefore, Eq. S5 now reads:

$$\varphi_1 - \varphi_2 = \varphi_{\text{ext}} + \frac{2\pi}{\Phi_0} (L'_2 I_2(\varphi_2) - L'_1 I_1(\varphi_1)). \quad (\text{S7})$$

Our simulations show, however, that the effect of the mutual inductance can be neglected in our experiment. Hence, there are six remaining parameters in the problem:  $I_{c1}$ ,  $I_{c2}$ ,  $\bar{\tau}_1$ ,  $\bar{\tau}_2$ ,  $L_1$ , and  $L_2$ . Since the appearance of the diode effect in a SQUID is related to asymmetries, we introduce three asymmetry parameters:

$$\alpha := \frac{I_{c1} - I_{c2}}{I_{c1} + I_{c2}}, \quad (\text{S8})$$

$$\beta := \frac{\bar{\tau}_1 - \bar{\tau}_2}{\bar{\tau}_1 + \bar{\tau}_2}, \quad (\text{S9})$$

$$\gamma := \frac{L_1 - L_2}{L_1 + L_2}. \quad (\text{S10})$$

The new set of parameters is now given by the three asymmetries and the mean critical current of the two junctions  $\bar{I}_c$ , the mean transmission probability  $\bar{\tau}$  and the mean inductance  $\bar{L}$ .

To find the critical current one has to find the maximum or minimum of the total supercurrent:

$$I(\varphi_1, \varphi_2) = I_1(\varphi_1) + I_2(\varphi_2). \quad (\text{S11})$$

Making use of Eq. S7, we get:

$$I(\varphi_1, I) = I_1(\varphi_1) + I_2(\varphi_1 - \varphi_{\text{ext}} + \kappa L_1 I_1(\varphi_1) - \kappa L_2 (I - I_1(\varphi_1))), \quad (\text{S12})$$

with  $\kappa = 2\pi/\Phi_0$ . In the latter form, we have eliminated  $\varphi_2$  using the fluxoid condition. However, due to the loop inductances, the equation for the total current  $I$  is now itself implicitly dependent on  $I$ . One can still solve this equation recursively or by introducing Lagrange multipliers to then search for the maximum or minimum currents, yielding  $I_c^+$  and  $I_c^-$ . [C. D. Tesche and J. Clarke, J. Low Temp. Phys. 29, 301-331 (1977)].

To find  $I_c^+$  numerically, we preset the value of  $I$ ,  $0 \leq I \leq 2\bar{I}_c$ , starting with a small one and search for solutions  $\varphi_1$  of Eq. S12. If solutions exist, we increment  $I$  by a small step  $\delta I$  until there are no solutions  $\varphi_1$  anymore. This defines now  $I_c^+$ . In analogy we obtain  $I_c^-$ .

## SVI. COMPARISON TO DIODE EFFECT BY LOOP INDUCTANCE

Here, we present a comparison of the measured critical currents  $I_c^+$  and  $I_c^-$  shown in Fig. 2c) with model simulations. Specifically, we discuss the effect of the loop inductance and its asymmetry on the diode effect. The comparison shows that the diode effect can poorly be reproduced taking only the loop inductances into account. This is shown in the following figure Fig. S5.

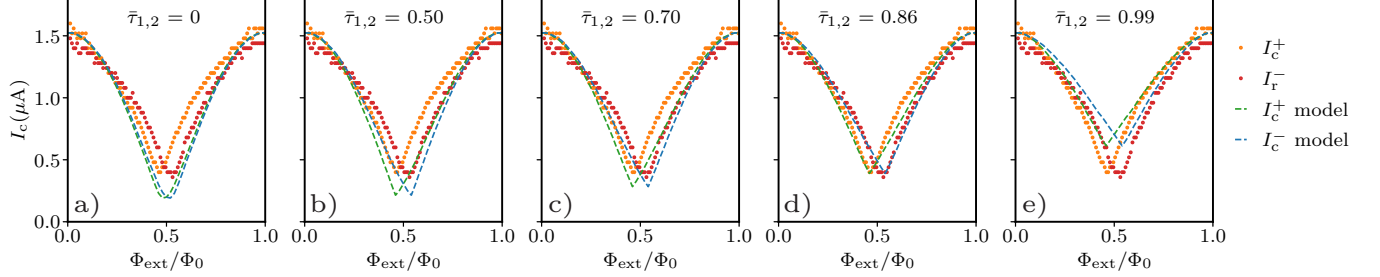


Figure S5. Sequence of simulations, blue and green dashed curves, to a set of measurements of  $I_c^+$  (orange) and  $I_c^-$  (red). In all five simulations the critical currents  $I_{c1}$  and  $I_{c2}$  of the two junctions are taken from the experiment, i.e. from Fig. 1c. Since  $V_{G1} = V_{G2} = 0$  we obtain  $I_{c1} = 0.87 \mu\text{A}$  and  $I_{c2} = 0.67 \mu\text{A}$ . In a) we assume sinusoidal CPRs for both junctions  $\text{JJ}_1$  and  $\text{JJ}_2$ , and we take the simulated loop inductances into account. Due to the slight asymmetry in loop inductance a small diode effect appears. However, this effect is far smaller than what has been measured. Hence, one cannot fit the measurement with the loop inductance asymmetry alone. In b)-e) we keep the loop inductances as estimated, but change to non-sinusoidal CPRs by increasing  $\bar{\tau}_1 = \bar{\tau}_2$  to appreciable values ranging from 0.5 – 0.99, indicated in the figures. As before, we obtain the blue and green dashed curves taking the known critical currents  $I_{c1}$  and  $I_{c2}$  of the two junctions. The best match is found for  $\bar{\tau}_1 = \bar{\tau}_2 \approx 0.86$ . One can see that the model matches the key feature of the experiment very well. However, there are deviations, as seen by the stronger curvature that the measurement points display as compared to the model. These differences are yet not understood.

## SVII. CONDITIONS FOR A DIODE EFFECT IN A SQUID DEVICE

The following three figures illustrate that an asymmetry is required to obtain a diode effect. In Fig. S6a) and b) sinusoidal CPRs are assumed. In a) the loop inductance asymmetry  $\gamma$  is varied, while  $\alpha = 0$ . In contrast, in b) the critical current asymmetry  $\alpha$  is varied, while  $\gamma = 0$ . A relatively large phase drop over the inductor of  $\varphi_L = 0.5$  has been assumed ( $\varphi_L = 4\pi\bar{I}_c\bar{I}_c\Phi_0$ ). In c) non-sinusoidal CPRs with different  $\bar{\tau}$  values,  $\beta \neq 0$ , are considered, while  $\alpha = \gamma = \varphi_L = 0$ .

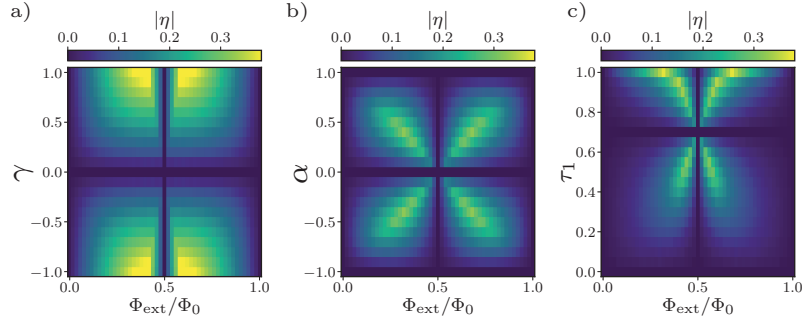


Figure S6. Magnitude of the diode efficiency  $|\eta|$  as a function of the applied external flux expressed in number of magnetic flux quanta  $\Phi_{\text{ext}}/\Phi_0$ , numerically calculated for an **asymmetry in loop inductance**  $\gamma$  at  $\varphi_L = \pi$ , b) an asymmetry in **critical current**  $\alpha$ . In c), we plot the magnitude of the calculated diode efficiency for  $\alpha = \gamma = \varphi_L = 0$ , and using  $A_i = 1$ ,  $N_i = 1$ ,  $\tau_2 = 0.7$ . This corresponds to a situation when there is no loop inductance, and each junction has only one channel with transparency  $\tau_1$ . In general, the diode efficiency is zero at the symmetry points, meaning for  $\Phi_{\text{ext}}/\Phi_0 = 0, \pi, 2\pi$ , and for  $\alpha = 0$ ,  $\gamma = 0$  and  $\tau_1 = \tau_2$ . Also, the position of maximum diode efficiency in flux depends on what kind of asymmetry dominates.



To obtain a diode effect in a SQUID loop, an asymmetry is required. This we have shown in the previous figure Fig. S6 where out of the three asymmetry parameters  $\alpha$ ,  $\beta$ ,  $\gamma$  only one was different from zero. In the following table we show under which conditions the diode effect appears depending on all three asymmetry parameters. The table shows that at least one symmetry has to be broken to get the DE effect. This is a sufficient condition for almost all cases. There is only one exception. It arises for sinusoidal CPRs where a difference in critical currents of the two junctions is not enough for a diode effect to appear.

Table II. Conditions for obtaining a diode effect (DE). In the first column  $\bar{\tau} = 0$  is used to refer to a sinusoidal CPR, while  $\bar{\tau} \neq 0$  indicates a highly transmissive CPR containing higher order terms in the CPR. If  $\bar{L} = 0$ , loop inductances are not considered, while they play a role in the entries where  $\bar{L} \neq 0$ .  $\alpha$  ( $\beta$ ) denotes the asymmetry in  $I_c$  ( $\bar{\tau}$ ) of the two JJs, while  $\gamma$  denotes the asymmetry in the loop inductances in the two arms the SQUID.

$\bar{\tau}$	$\beta$	$\alpha$	$\bar{L}$	$\gamma$	DE
0	n.a.	0	0	n.a.	no
0	n.a.	0	$\neq 0$	0	no
0	n.a.	0	$\neq 0$	$\neq 0$	yes
0	n.a.	$\neq 0$	0	n.a.	no
0	n.a.	$\neq 0$	$\neq 0$	0	yes
0	n.a.	$\neq 0$	$\neq 0$	$\neq 0$	yes
$\neq 0$	0	0	0	n.a.	no
$\neq 0$	0	0	$\neq 0$	0	no
$\neq 0$	0	0	$\neq 0$	$\neq 0$	yes
$\neq 0$	0	$\neq 0$	0	n.a.	yes
$\neq 0$	0	$\neq 0$	$\neq 0$	0	yes
$\neq 0$	0	$\neq 0$	$\neq 0$	$\neq 0$	yes
$\neq 0$	$\neq 0$	0	0	n.a.	yes
$\neq 0$	$\neq 0$	0	$\neq 0$	0	yes
$\neq 0$	$\neq 0$	0	$\neq 0$	$\neq 0$	yes
$\neq 0$	$\neq 0$	$\neq 0$	0	n.a.	yes
$\neq 0$	$\neq 0$	$\neq 0$	$\neq 0$	0	yes
$\neq 0$	$\neq 0$	$\neq 0$	$\neq 0$	$\neq 0$	yes